Influence of aspect ratio, plasma viscosity, local magnetic shear, and radial location of the q=1 resonant surface on the plasmoid formation in the low resistivity plasma in Tokamak

W. Zhang[1*], Z. W. Ma[1,*], H. W. Zhang[1], W. J. Chen[1], and X. Wang[1]

[1]Institute for Fusion Theory and Simulation, Department of Physics, Zhejiang University, Hangzhou 310027, China

Abstract: In the present paper, we systematically investigate the nonlinear evolution of the resistive kink mode in the low resistivity plasma in Tokamak geometry. We find that the aspect ratio of the initial equilibrium can significantly influence the critical resistivity for plasmoid formation. In Tokamaks with the aspect ratio of 3/1, the critical resistivity can be one magnitude larger than that in cylindrical geometry with the development of high n modes due to the strong mode-mode coupling. We also find that several initial parameters can largely influence the formation of plasmoids, i.e., the critical resistivity for plasmoid formation η_{crit} decreases with increasing plasma viscosity, or the magnetic shear on the q=1 resonant surface, or the decreasing radial location of the q=1 resonant surface.

*) Corresponding Authors: wzhang_ifts@zju.edu.cn and zwma@zju.edu.cn

I. Introduction

It is widely accepted that a thin current sheet forms during magnetic reconnection and may be unstable to the secondary tearing instability when the plasma resistivity is sufficiently low.[1-8] The secondary tearing instability in the thin current sheets might lead to fast reconnection phenomena both in space[2, 4, 9-18] and Tokamak plasma[19-27]. During the development of the secondary tearing instability, the current sheet breaks up, and multiple X-point reconnection takes place, [28] which results in the formation of multiple secondary islands or the so-called 'plasmoids'.

These multiple secondary islands often merge into a larger secondary island finally. The formation of large secondary islands sometimes can significantly influence the nonlinear behavior of the non-ideal MHD instabilities in Tokamak, especially the resistive-kink mode.[29, 30] As shown by Q. Yu et al., [31] the nonlinear behavior of the resistive kink mode can be qualitatively different from the well-known Kadomtsev's reconnection model[32]. With a sufficient low plasma resistivity, a thin current sheet forms along with the development of the resistive kink mode, and eventually becomes unstable to the secondary tearing instability when the width of the current sheet is thinner than a critical value. The current sheet then breaks up, and several secondary islands form and later merge into a large secondary island. If the width of this secondary island is large enough, it can stop the further development of the resistive kink mode, and the main m/n=1/1 magnetic island cannot expand to occupy the whole central core region as it does in Kadomtsev's reconnection model. As a result, incomplete reconnection occurs.

Yu's incomplete reconnection model is important for understanding the incomplete reconnection process observed in Tokamaks[33-38]. But, they carried out the simulation studies using the cylindrical geometry reduced MHD code.[31] In our previous studies, we have focused on the symmetry breaking introduced by the two-fluids effect, the shear flows, and the asymmetric initial perturbations. [waiting for the link of our previous work] However, the threshold of the plasmoids formation has not been solved yet. In the present paper, we will focus on this problem and systematically investigate the influence of aspect ratio, the plasma viscosity, the radial location, and the local magnetic shear of the q=1 resonant surface on the critical resistivity for the plasmoid formation through the 3D toroidal nonlinear full-MHD code CLT.[39, 40]

The remainder of the paper is organized as follows: in Section II, we briefly introduce the physical model used in our simulations. In Section III. A, we investigate the influence of the plasma resistivity on the nonlinear evolution of the resistive kink mode and find that there is a critical resistivity for plasmoid formation. After that, we systematically investigate the influence of the aspect ratio, the plasma viscosity, the

magnetic shear, and the radial location of the q=1 resonant surface on the critical resistivity for plasmoid formation in Section III. B, C, and D, E. A detailed discussion has been given in Section IV.

II. Numerical model

The 3D toroidal full-MHD equations used in CLT code are given as follows:

$$\frac{\partial \rho}{\partial t} = -\nabla \cdot (\rho \mathbf{v}) + \nabla \cdot [D \nabla (\rho)], \tag{1}$$

$$\frac{\partial p}{\partial t} = -\mathbf{v} \cdot \nabla p - \Gamma p \nabla \cdot \mathbf{v} + \nabla \cdot [\kappa_{\perp} \nabla (p - p_0)] + \nabla \cdot [\kappa_{\parallel} \nabla_{\parallel} p], \tag{2}$$

$$\frac{\partial \mathbf{v}}{\partial t} = -\mathbf{v} \cdot \nabla \mathbf{v} + (\mathbf{J} \times \mathbf{B} - \nabla p) / \rho + \nabla \cdot [\nu \nabla (\mathbf{v})], \tag{3}$$

$$\frac{\partial \mathbf{B}}{\partial t} = -\nabla \times \mathbf{E}, \tag{4}$$

$$\mathbf{E} = -\mathbf{v} \times \mathbf{B} + \eta (\mathbf{J} - \mathbf{J}_0), \tag{5}$$

$$\mathbf{J} = \nabla \times \mathbf{B}, \tag{6}$$

where ρ, p, $\mathbf{v}$, $\mathbf{B}$, $\mathbf{E}$ and $\mathbf{J}$ are the plasma density, the plasma pressure, the fluid velocity, the magnetic field, the electric field and, the current density, respectively. The subscript "0" indicates their initial values. The ratio of specific heat is $\Gamma = 5/3$. η, D, $\kappa_{\perp}$, $\kappa_{\parallel}$, and υ are the plasma resistivity, the diffusion coefficient, the perpendicular, and parallel thermal conductivities, and the plasma viscosity, respectively.

In CLT code, all the variables are normalized as follows: $\mathbf{x}/a \to \mathbf{x}$, $t/t_A \to t$, $\rho/\rho_{00} \to \rho$, $p/(B_{00}^2/\mu_0) \to p$, $\mathbf{v}/v_A \to \mathbf{v}$, $\mathbf{B}/B_{00} \to \mathbf{B}$, $\mathbf{E}/(v_A B_{00}) \to \mathbf{E}$, $\mathbf{J}/(B_{00}/\mu_0 a) \to \mathbf{J}$, $\eta/(\mu_0 a^2/t_A) \to \eta$, $D/(a^2/t_A) \to D$, $\kappa_{\perp}/(a^2/t_A) \to \kappa_{\perp}$, $\kappa_{\parallel}/(a^2/t_A) \to \kappa_{\parallel}$, and $\nu/(a^2/t_A) \to \nu$, respectively. a is the minor radius, $v_A = B_{00}/\sqrt{\mu_0 \rho_{00}}$ is the Alfvén speed, and $t_A = a/v_A$ is the Alfvén time, where B_{00} and ρ_{00} are the initial magnetic field and the plasma density at the magnetic axis, respectively.

In CLT, the electric field is chosen to be an intermediate variable for the sake of keeping divergence B free. CLT's numerical scheme is the 4th order finite difference

method for the spatial derivatives and the 4th order Runge–Kutta scheme for the time integration. We choose the cut-cell method to handle the boundary problems since the physical boundary is not located at the grids [41]. In the present paper, the fixed boundary condition is used for all the variables. The uniform meshes with ($400\times64\times400$) in (R,φ,Z) are used in all the simulations. A systematical benchmark between the CLT code and the M3D-C1 code is given in Ref. [39].

III. Simulation results

A. The influence of plasma resistivity on the nonlinear behavior of the resistive-kink mode

In this subsection, we choose the same initial equilibrium with our previous studies[waiting for the link of our previous work], which is shown in Figure 1. The q profile function is given in Equation (7):

$$q = q_0 \times (1 + (\psi / q_1)^{q_2})^{\frac{1}{q_2}} \tag{7}$$

where $q_0 = 0.9$, $q_1 = 1.0$, and $q_2 = 1.0$, respectively. For simplification, the plasma beta used in the simulations is assumed to be $\beta \sim 0$. The initial equilibrium is derived by the Qsolver included in the NOVA code [42]. When deriving the equilibrium, we chose a Tokamak configuration with the aspect ratio of $R_0 / a = 3/1$, which is close to ASDEX-U. [43]

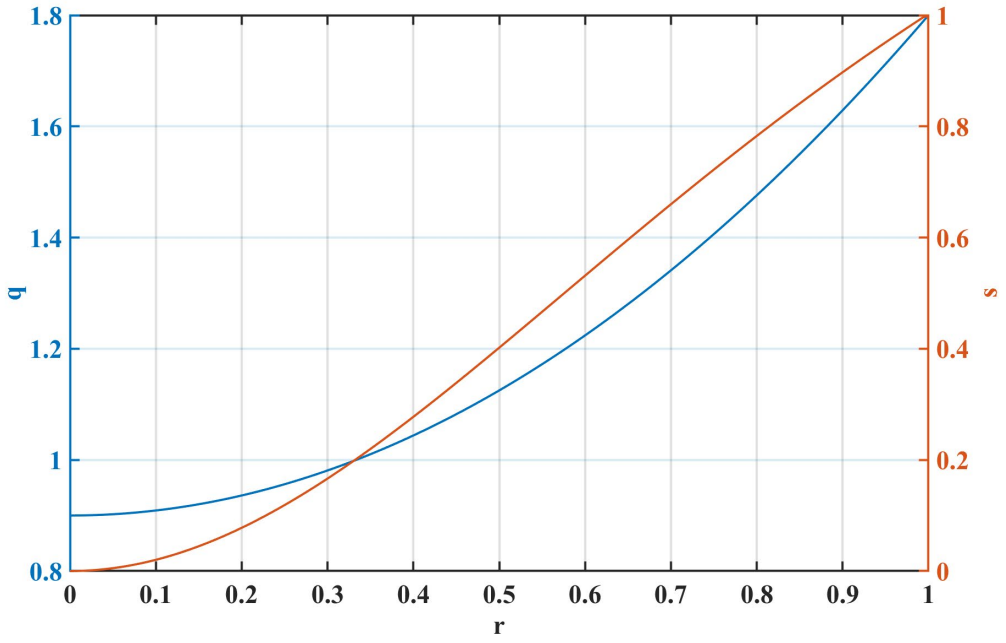

Figure 1 Profiles of the initial safety factor q and the corresponding magnetic shear

($s = \frac{r}{q}\frac{dq}{dr}$). The radial position and the local magnetic shear of the q=1 resonant surface are $r_1 = 0.34$ and $s_1 = 0.2$, respectively.

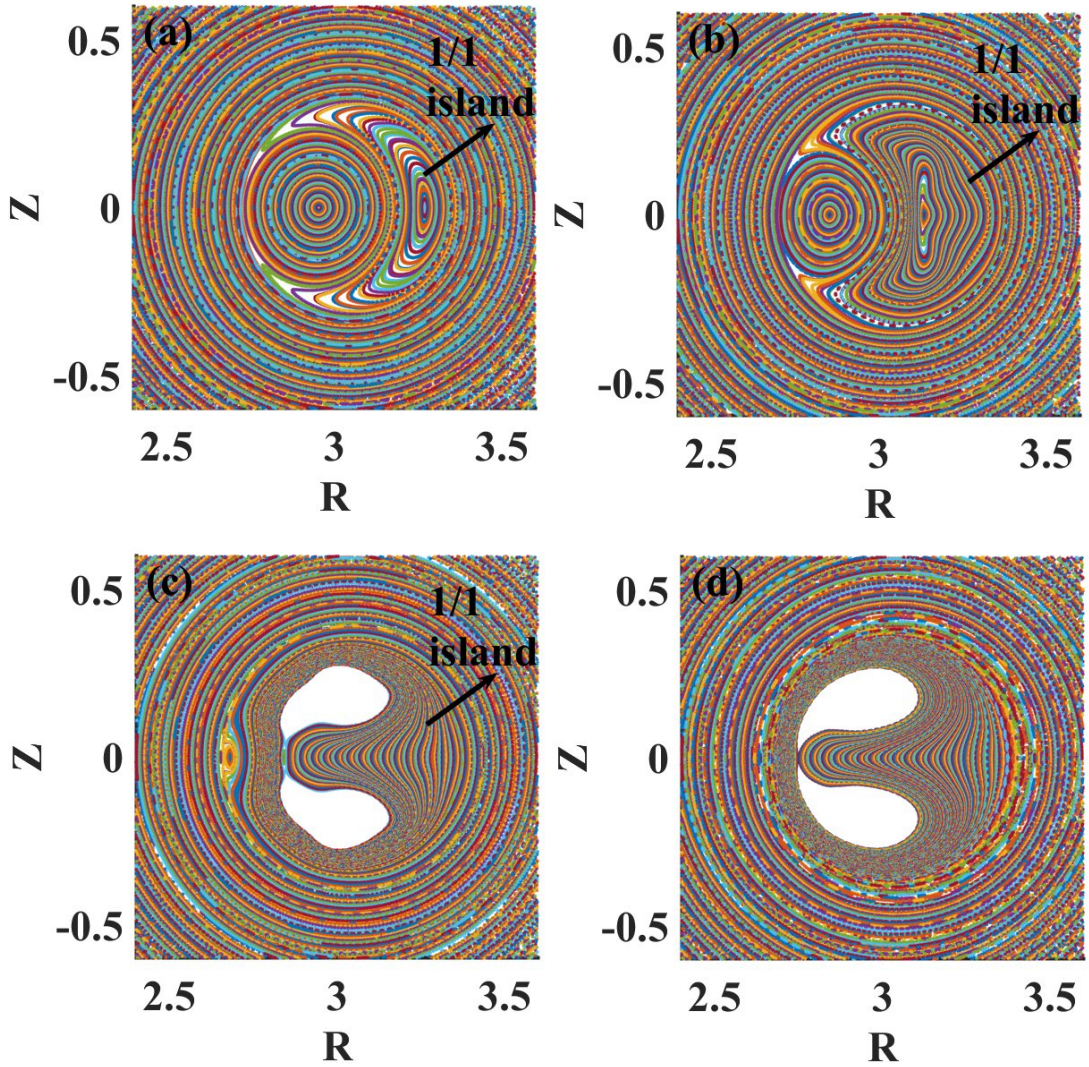

Figure 2 Four snapshots of Poincare plots of the magnetic field with a relatively high resistivity (η=3.0×10^{-6}).

To investigate the influence of the plasma resistivity on the nonlinear behavior of the resistive-kink mode, we scan the resistivity from η=1.0×10^{-5} to η=1.0×10^{-7}, and other parameters are chosen to be $D = 1.0\times10^{-4}$, $\kappa_\perp = 3.0\times10^{-6}$, $\kappa_\parallel = 5.0\times10^{-2}$, and

ν=3.0×10^{-7} . (It should be noted that since the plasma beta β~0 , the thermal conductivities $\kappa_{\perp}$ and $\kappa_{\parallel}$ has no influence on the simulation results.) We find that the nonlinear evolutions of the resistive kink mode can be qualitatively different with different resistivities.

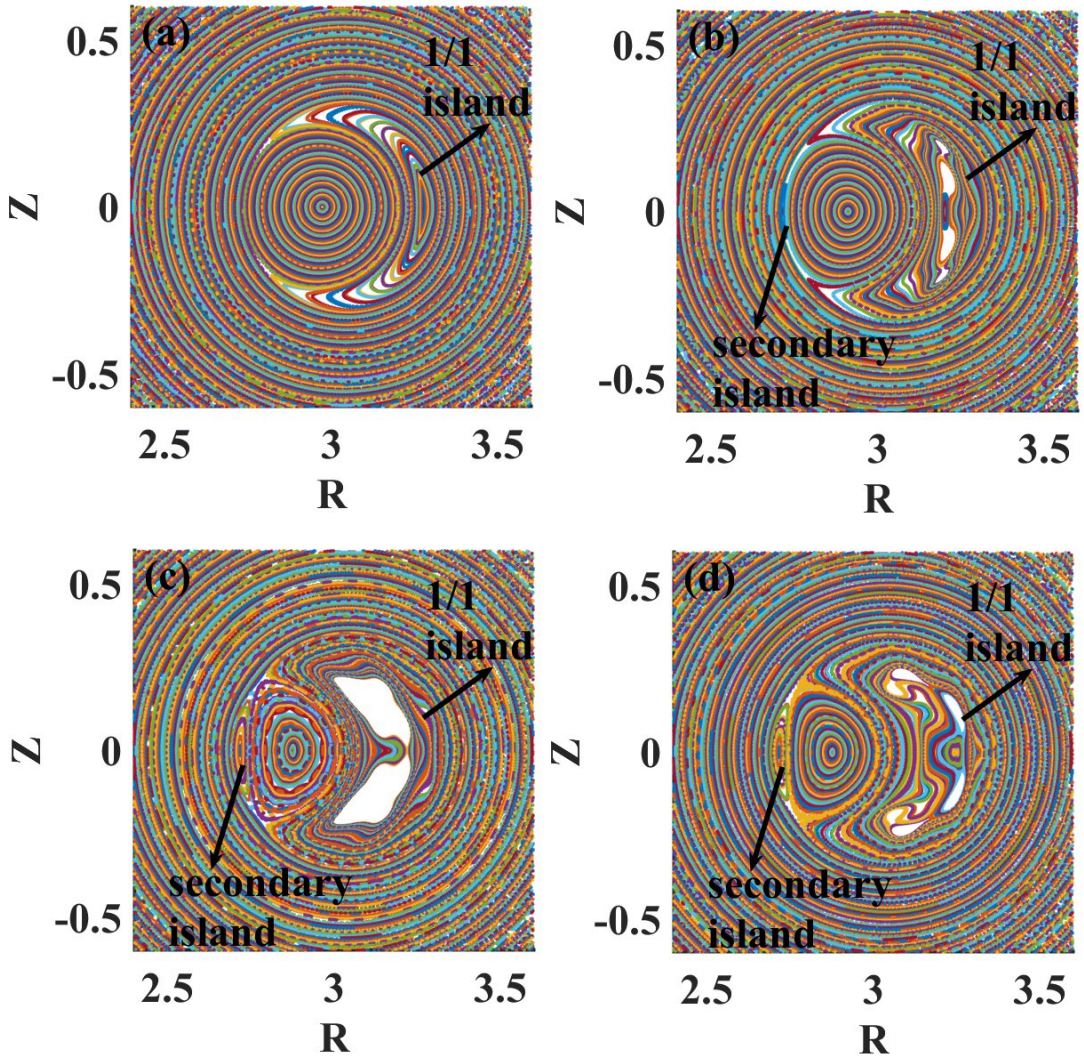

Figure 3 Four snapshots of Poincare plots of the magnetic field for the case with a relatively low resistivity (η=5.0×10^{-7}).

Poincare plots of the magnetic field with a relatively high resistivity (η=3.0×10^{-6}) are shown in Figure 2. The m/n=1/1 magnetic island continues to grow up and finally occupies the whole core region, which is consistent with the process proposed by

Kadomtsev.[32] However, with a sufficiently low resistivity (i.e., $\eta=5.0\times10^{-7}$), the nonlinear behavior significantly differs from that predicted the Kadomtsev's theory. As shown in Figure 3, a large secondary island forms at the nonlinear stage. The formation of the large secondary island is due to the secondary tearing instability inside the thin current sheet. During the nonlinear evolution of the resistive-kink mode, the current sheet becomes thinner and thinner. When the ratio of the length and the thickness of the current sheet exceeds a critical value (typically ~60[31]), the current sheet will be unstable to the secondary island instability and multiple X-line reconnection occur.[28] During the multiple X-line reconnection, secondary islands form and the current sheet breaks into several parts. The contour plots of toroidal current density at four typical moments are shown in Figure 4, which tells the same story as Figure 3. Finally, these small secondary islands merge into a large secondary island, and finally prevent the further development of the resistive-kink mode, leading to the incomplete reconnection. It is clear that the nonlinear behavior is qualitatively different from the complete reconnection model.[32] With an intermediate resistivity (i.e., $\eta=1.0\times10^{-6}$), we find that the secondary tearing instability can also be unstable. But the ratio of the length and the thickness of the current sheet is not as large as it is in the case with the low resistivity, and the secondary island is rather small as shown in Figure 5. In this case, the secondary island is too small to prevent the further development of the main m/n=1/1 island, and the m/n=1/1 island finally occupies the whole core region and causes complete reconnection.

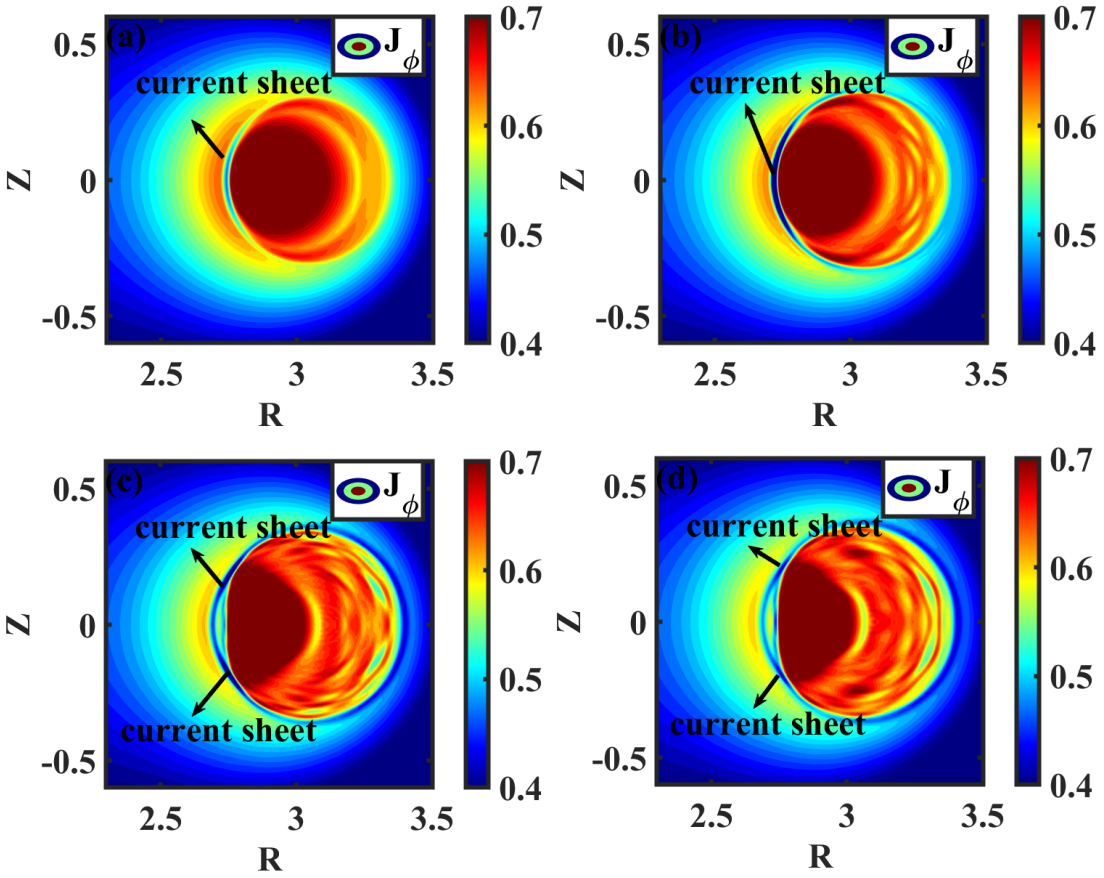

Figure 4 The contour plots of the toroidal current density at the four typical moments ((a) $t = 3327t_A$ when a thin current forms, (b) $t = 3708t_A$ when the current sheet is thin enough to become unstable to the secondary tearing instability, (c) $t = 4088t_A$ when multiple X-line reconnection occurs and the current sheet breaks into several parts, and (d) $t = 4278t_A$ when a large secondary island forms).

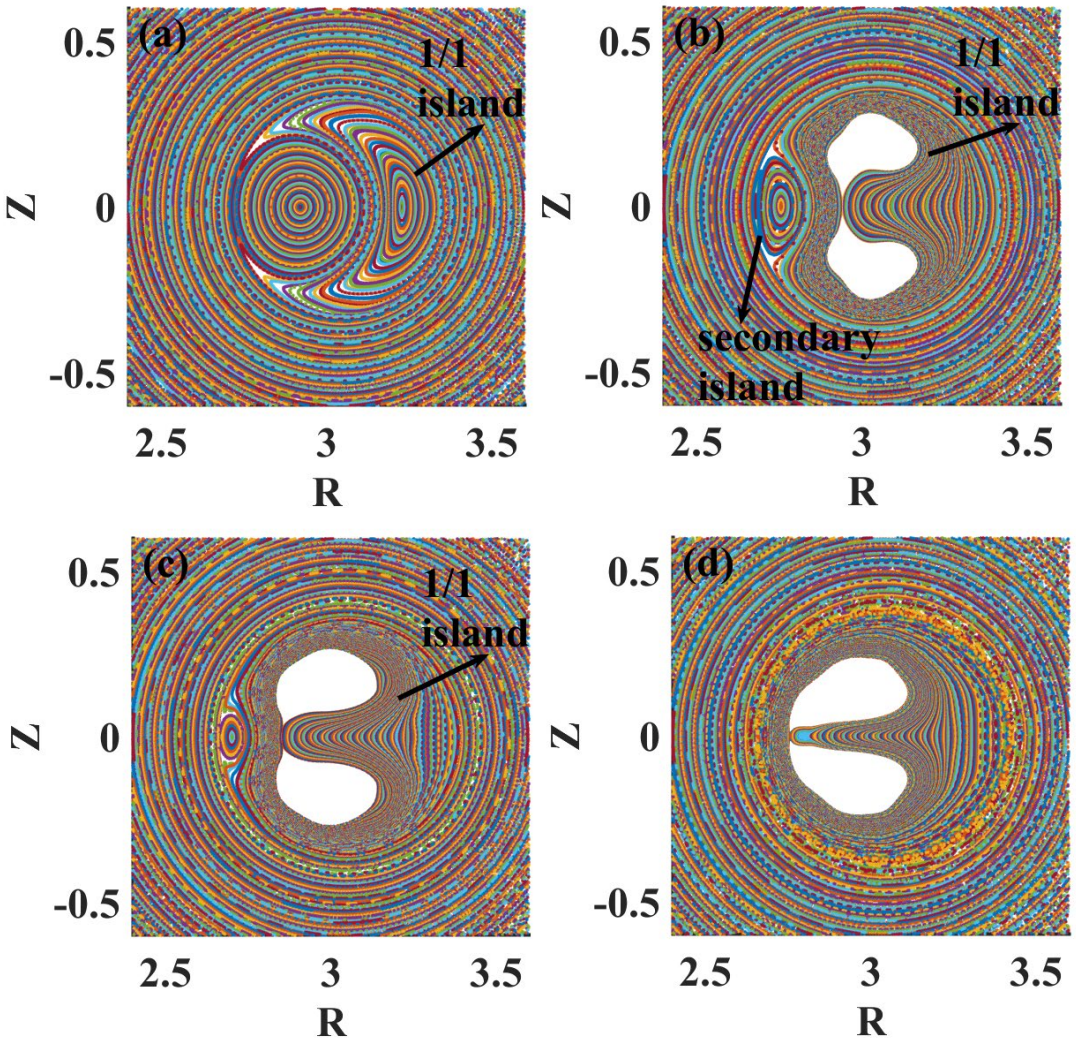

Figure 5 Four snapshots of Poincare plots of the magnetic field for the case with an intermediate resistivity (η=1.0×10^{-6}).

The maximum (w_M) and saturated width (w_S) of the main m/n=1/1 magnetic island as a function of η are shown in Figure 6. For the case with $\eta \geq 3.0\times10^{-6}$, the maximum width of the main m/n=1/1 island is the radial width of the mix region ($w_M = r_{mix} = 0.37$), which is slightly larger than $r_1 = 0.34$ (the radial width of the $q < 1.0$ region). Since a part of magnetic flux inside the mix region has been reconnected during the formation of the secondary island, the maximum width of the main 1/1 island will be larger than r_{mix} (for the case with η=1.0×10^{-6}, the maximum width is $w_M = 0.41$).

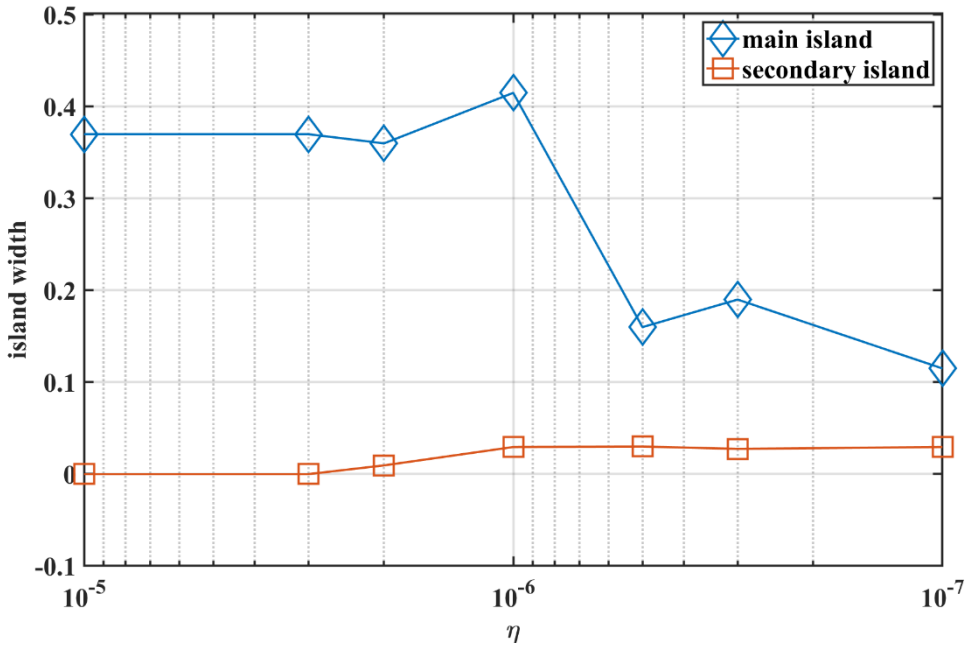

Figure 6 The maximum or saturated width of the main m/n=1/1 magnetic island as a function of η.

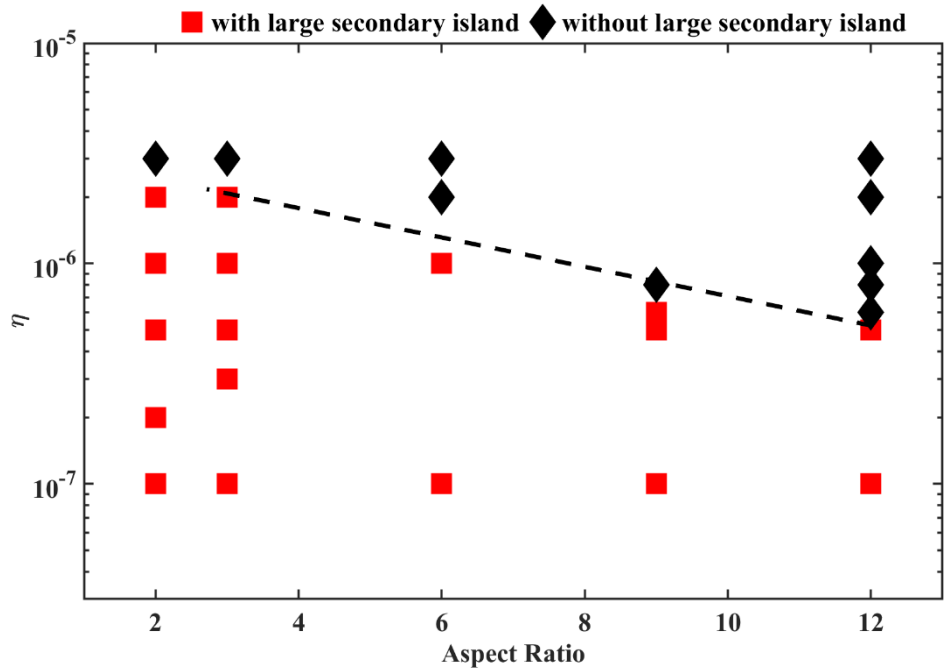

Figure 7 The influence of the plasma resistivity and the aspect ratio on plasmoid formation. The red square/the black diamond represents with/without large secondary island.

B. The influence of the aspect ratio of Tokamaks on the critical resistivity for plasmoid formation

As shown in Section III. A, plasmoids can form during the nonlinear evolution of the resistive kink mode if the plasma resistivity is smaller than the critical resistivity $\eta_{crit} = 3\times10^{-6}$. It should be noted that $\eta_{crit} = 3\times10^{-6}$ in Section III. A is at least one magnitude larger than that from Yu's previous work, in which the critical resistivity is $\eta_{crit} = 3\times10^{-7}$ (Figure 4 in Ref. [31]). The large difference implies that there must be some physical parameters that can largely influence the plasmoid formation. Note that, Yu's work is carried out under a periodic cylindrical geometry, in which the large aspect ratio assumption is adopted; while the aspect ratio of the initial equilibrium is only $3/1$ in Section III. A. This might be the reason for the large difference in the critical resistivity for plasmoid formation.

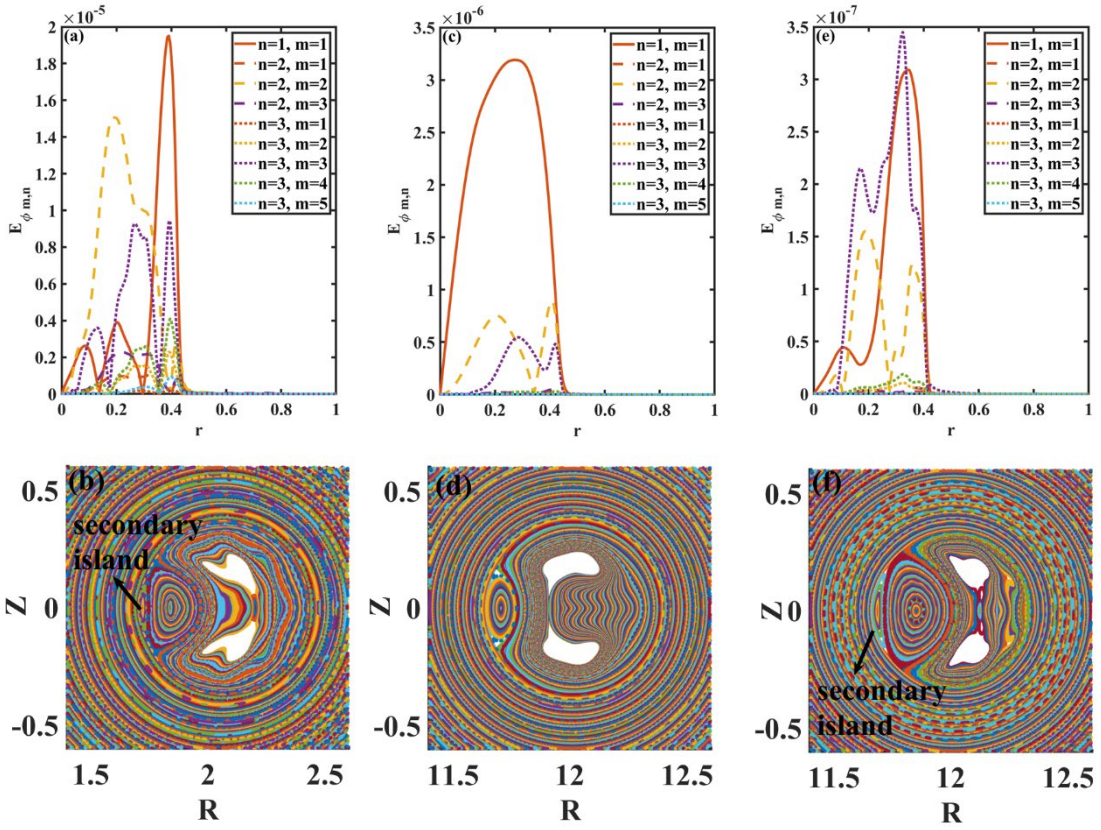

Figure 8. (a) The Fourier components of the perturbed toroidal electric field E_φ and (b) the corresponding Poincare plots of the magnetic field lines with the aspect ratio $R_0/a = 2/1$ and $\eta = 1\times10^{-6}$. (c) The Fourier components of the perturbed toroidal electric field E_φ and (d) the corresponding Poincare plots of the magnetic field lines

with the aspect ratio $R_0/a=12/1$ and $\eta=1\times10^{-6}$. (e) The Fourier components of the perturbed toroidal electric field E_φ and (f) the corresponding Poincare plots of the magnetic field lines with the aspect ratio $R_0/a=12/1$ and $\eta=1\times10^{-7}$.

In this subsection, we scan the aspect ratio to investigate its influence on the critical resistivity for plasmoid formation. A series of Tokamak equilibriums with different aspect ratios 2/1, 3/1, 6/1, 9/1, and 12/1 from the NOVA[42] code is chosen to be the initial conditions and other parameters are chosen to be $D=1.0\times10^{-4}$, $\kappa_\perp=3.0\times10^{-6}$, $\kappa_\parallel=5.0\times10^{-2}$, and ν=1.0×10^{-7}. The influence of the plasma resistivity and the aspect ratio on plasmoid formation is shown in Figure 7. As we can see, the critical resistivity η_{crit} decrease with increasing aspect ratio. For a large aspect ratio (~12), the critical resistivity is about $\eta_{crit}\sim5\times10^{-7}$, which is close to Yu's simulation results in the periodic cylindrical geometry.

The large difference in the critical resistivity with different aspect ratios of Tokamaks indicates that the toroidal effect plays an important role in the formation of plasmoids. Since the toroidal effect mainly affects the strength of the mode-mode coupling, we can analyze the perturbations through the Fourier transform method to see how the toroidal effect works. The Fourier components of the perturbed toroidal electric field E_φ and the corresponding Poincare plots of the magnetic field lines with the aspect ratio $R_0/a=2/1$ and $\eta=1\times10^{-6}$ (with a large secondary island) are shown in Figure 8 (a) and (b). For comparison, the Fourier components of the perturbed toroidal electric field E_φ and the corresponding Poincare plots of the magnetic field lines with the aspect ratio $R_0/a=12/1$ and $\eta=1\times10^{-6}$ (without a large secondary island) are shown in Figure 8 (c) and (d). Without large secondary island formation, the m/n=1/1 resistive-kink mode remains dominant throughout the simulations. In the meanwhile, other visible modes are only the harmonics of the m/n=1/1 mode: the m/n=2/2 and m/n=3/3 modes and their amplitudes are much smaller than that of the m/n=1/1 mode. However, with large secondary island formation, the amplitude of the m/n=2/2 and m/n=3/3 modes can be as large as the m/n=1/1 mode. The Fourier components of the perturbed toroidal electric field E_φ and the corresponding Poincare

plots of the magnetic field lines with the aspect ratio $R_0 / a = 12/1$ and $\eta = 1\times10^{-7}$ (with a large secondary island) are shown in Figure 8 (e) and (f). Figure 8 (e) and (f) also confirm that the amplitude of the m/n=2/2 and m/n=3/3 modes can be larger than or at least comparable to the m/n=1/1 mode, but other non-harmonic modes are not present as the small aspect ratio shown in Figure 8(a). This is because, with a small aspect ratio $R_0 / a = 2/1$, the toroidal effect is strong and the mode with $(m\pm1, n)$ will be generated by the (m, n).[44] However, with a large aspect ratio, the toroidal effect is weak and the $(m\pm1, n)$ cannot be generated. It is clear that the toroidal effect is helpful for the development of high n modes. This is why the large secondary island can be more easily to form with a small aspect ratio.

C. The influence of the plasma viscosity on the critical resistivity for plasmoid formation

As we all know, the spatial scale of the secondary tearing instability is much smaller than the kink instability, and the secondary tearing instability should be more sensitive to the plasma viscosity. In this subsection, we scan the plasma viscosity from ν=1.0×10^{-7} to ν=1.0×10^{-5} and investigate the influence of plasma viscosities on η_{crit} for plasmoid formation. The influence of the plasma resistivity and viscosity on plasmoid formation is shown in Figure 9. The critical resistivity η_{crit} decreases with increasing ν, which indicates that plasmoids is much difficult to form with a larger viscosity. Note that the formation of plasmoid results from the secondary tearing instability, and the secondary tearing instability is sensitive to the plasma viscosity. With a larger viscosity, the secondary tearing instability is more difficult to develop, which is why η_{crit} decreases with increasing ν. The influence of the Prandtl number $\mathrm{Pr} = \nu / \eta$ on η_{crit} for plasmoid formation is shown in Figure 10. Similarly, it indicates that the critical resistivity η_{crit} decreases with increasing Pr. However, if $\mathrm{Pr} < 0.1$ (i.e., the system approaches the low viscosity limit), the Prandtl number does not influence the critical resistivity for plasmoid formation. In this subsection, the Prandtl number is kept from $0.01 < \mathrm{Pr} < 100$ that covers the parameter regime for Tokamak plasma.

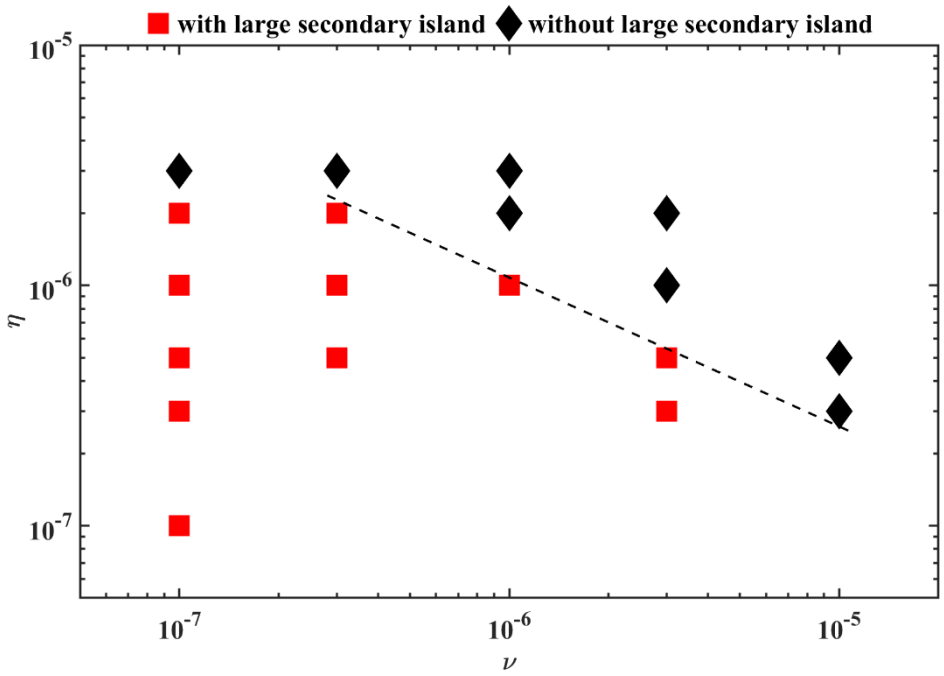

Figure 9 The influence of the plasma resistivity and viscosity on plasmoid formation. The red square/the black diamond represents with/without large secondary island formation in this simulation.

Similar to what we have done in Section III. B, we use the Fourier transform method to analyze the modes. The Fourier components of the perturbed toroidal electric field E_φ and the corresponding Poincare plots of the magnetic field lines with $\nu = 1\times10^{-7}$ and $\eta = 1\times10^{-6}$ (with large secondary island formation) are shown in Figure 11 (a) and (b). For comparison, the case with viscosity $\nu = 3\times10^{-6}$ and $\eta = 1\times10^{-6}$ is shown in Figure 11 (c) and (d), in which no large secondary island has been observed. The case with viscosity $\nu = 3\times10^{-6}$ and $\eta = 1\times10^{-7}$ is shown in Figure 11 (e) and (f). With much lower resistivity, the current sheet can be much thinner, and the secondary tearing instability can be much unstable. As a result, the secondary tearing instability can grow up in high viscosity system, and then the large secondary island forms. The plasmoids are much easier to form in the low viscosity system and harder to form in the high viscosity system.

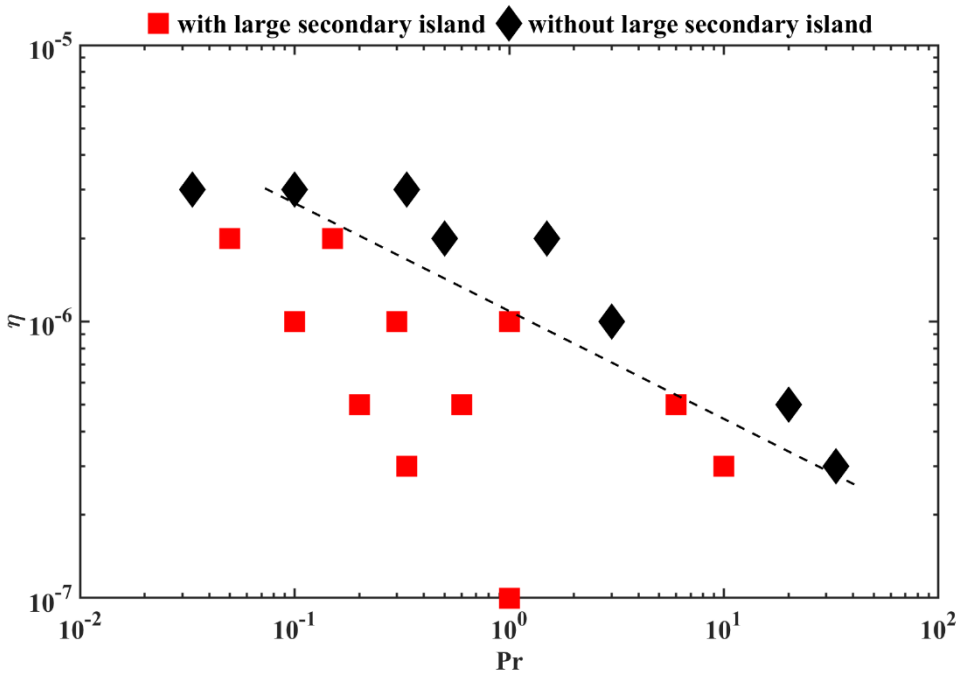

Figure 10 The influence of the Prandtl number and the resistivity on plasmoid formation. The red square/the black diamond represents with/without large secondary island formation in this simulation.

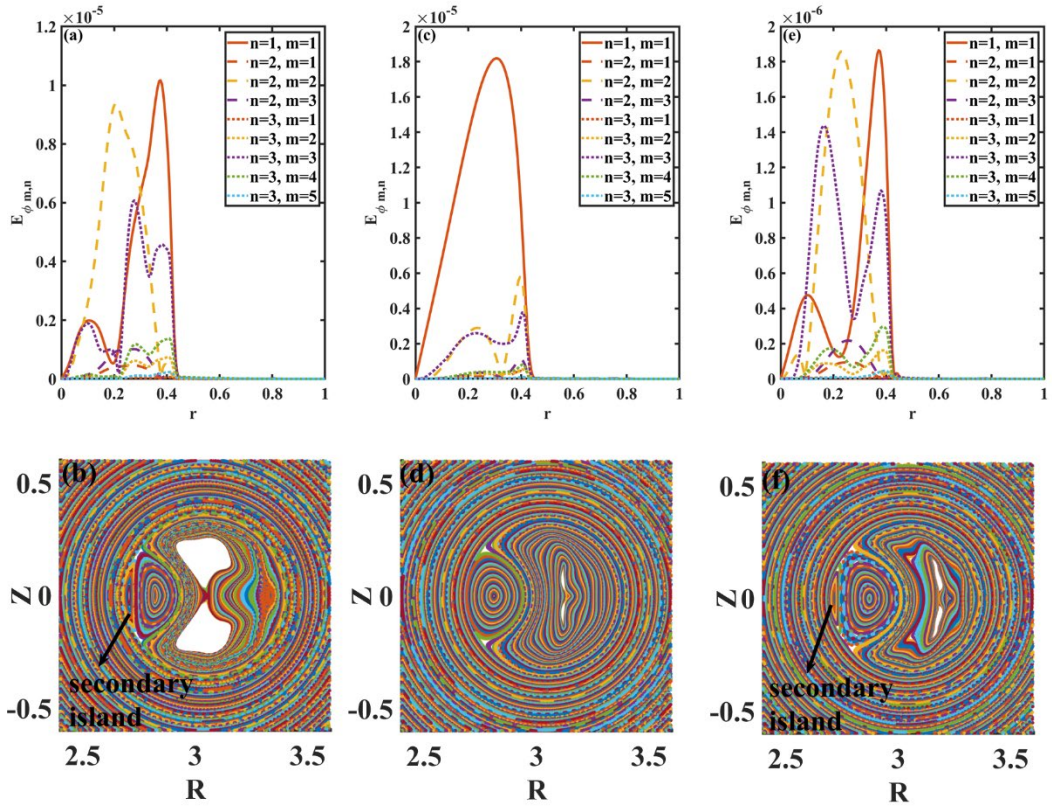

Figure 11 (a) and (b): the Fourier components of the perturbed toroidal electric field

E_φ and the corresponding Poincare plots of the magnetic field lines with aspect ratio $\nu = 1\times10^{-7}$ and $\eta = 1\times10^{-6}$. (c) and (d): the Fourier components of the perturbed toroidal electric field E_φ and the corresponding Poincare plots of the magnetic field lines with aspect ratio $\nu = 3\times10^{-6}$ and $\eta = 1\times10^{-6}$. (e) and (f): the Fourier components of the perturbed toroidal electric field E_φ and the corresponding Poincare plots of the magnetic field lines with aspect ratio $\nu = 3\times10^{-6}$ and $\eta = 1\times10^{-7}$.

D. The influence of local magnetic shear on the critical resistivity for plasmoid formation

In this subsection, we investigate the influence of the magnetic shear on the q=1 resonant surface (s_1) on the critical resistivity for plasmoid formation. Through Eq. (7), we can set up a series of the equilibria with $r_1 = 0.34$, $q_0 = 0.9$, but different s_1, i.e., $s_1 = 0.2$, $s_1 = 0.3$, and $s_1 = 0.4$, respectively. The initial q profiles are shown in Figure 12.

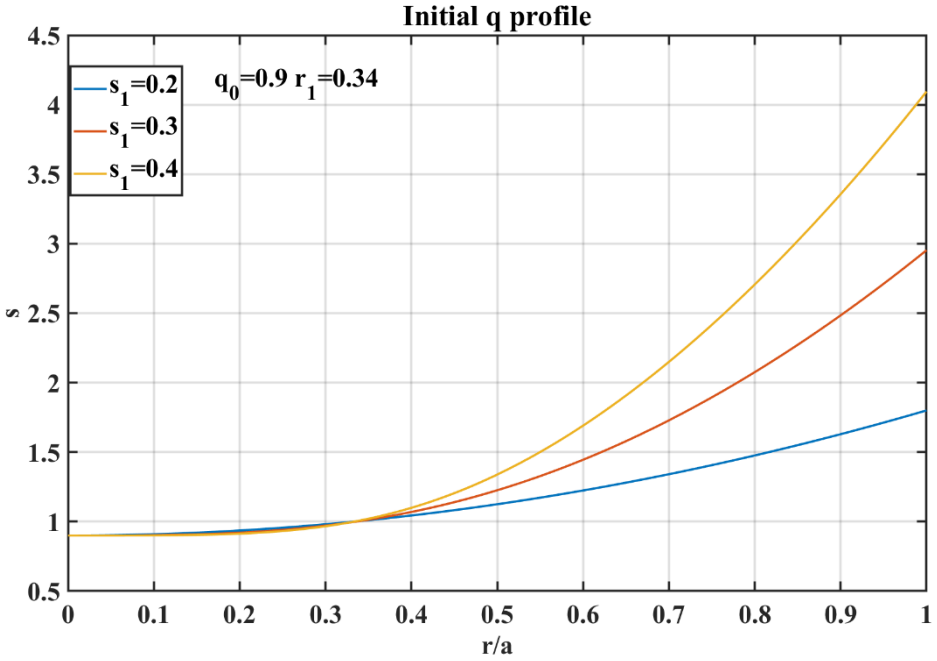

Figure 12 The initial q profiles with $r_1 = 0.34$, $q_0 = 0.9$, but $s_1 = 0.2$, $s_1 = 0.3$, and

$s_1 = 0.4$.

With these initial equilibria, we scan the resistivity from η=1.0×10^{-5} to η=1.0×10^{-7}, and other parameters are chosen to be $D = 1.0\times10^{-4}$, $\kappa_{\perp} = 3.0\times10^{-6}$, $\kappa_{\parallel} = 5.0\times10^{-2}$, and ν=3.0×10^{-7}. The influence of the local magnetic shear and the resistivity on the plasmoid formation is shown in Figure 13. It is found that the critical resistivity η_{crit} decreases with increasing the local magnetic shear s_1. Note that, the growth rate of the resistive kink mode increases with increasing s_1. It means the larger s_1 is, the faster the resistive kink mode develops, the shorter time duration the secondary tearing instability develops, and the harder a visible secondary island forms in the simulations.

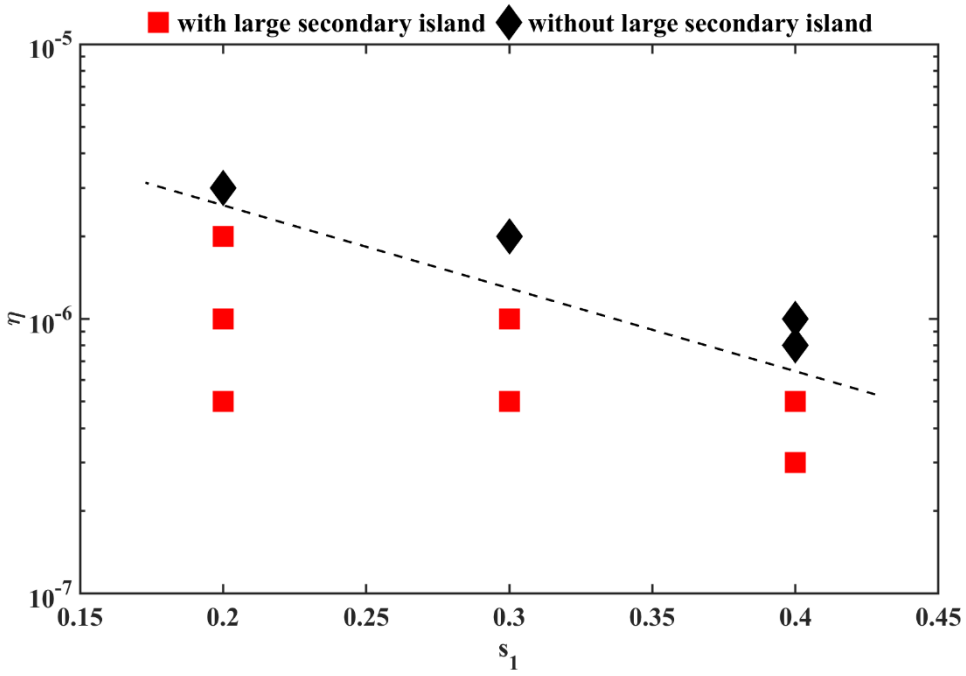

Figure 13 The influence of the local magnetic shear and the resistivity on plasmoid formation. The red square/the black diamond represents with/without large secondary island formation in this simulation.

E. The influence of the radial location of the q=1 resonant surface on the critical resistivity for plasmoid formation

Following the procedure in Section III. D, we investigate the influence of the radial

location of the q=1 resonant surface (r_1) on the critical resistivity for plasmoid formation. Through Eq. (7), we can set up a series of equilibrium with $q_0 = 0.9$, $s_1 = 0.2$, but different r_1, i.e., $r_1 = 0.237$, $r_1 = 0.284$, $r_1 = 0.336$, and $r_1 = 0.39$, respectively. The initial q profiles and the corresponding magnetic shear profiles are shown in Figure 14.

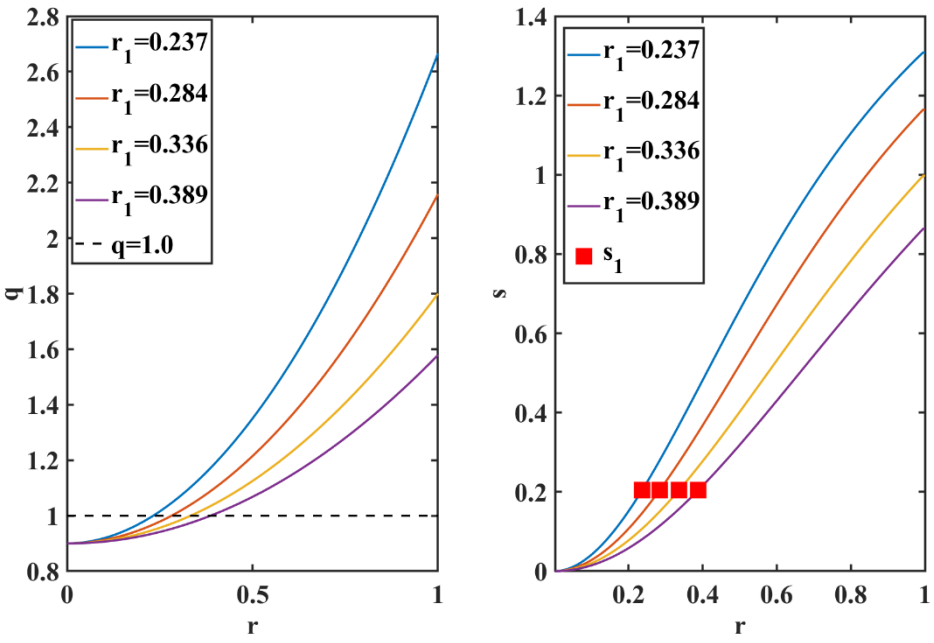

Figure 14 The initial q profiles and the corresponding magnetic shear profiles with $q_0 = 0.9$, $s_1 = 0.2$, but different r_1, i.e., $r_1 = 0.237$, $r_1 = 0.284$, $r_1 = 0.336$, and $r_1 = 0.39$. The red square in the right figure indicates the magnetic shear on the q=1 resonant surface for each equilibrium.

With these initial equilibria, we scan the resistivity from η=1.0×10^{-5} to η=1.0×10^{-7}, and other parameters are chosen to be $D = 1.0\times10^{-4}$, $\kappa_\perp = 3.0\times10^{-6}$, $\kappa_\parallel = 5.0\times10^{-2}$, and ν=3.0×10^{-7}. The influence of the location of the q=1 resonant surface and the resistivity on plasmoid formation is shown in Figure 15. The critical resistivity η_{crit} increase with increasing r_1.

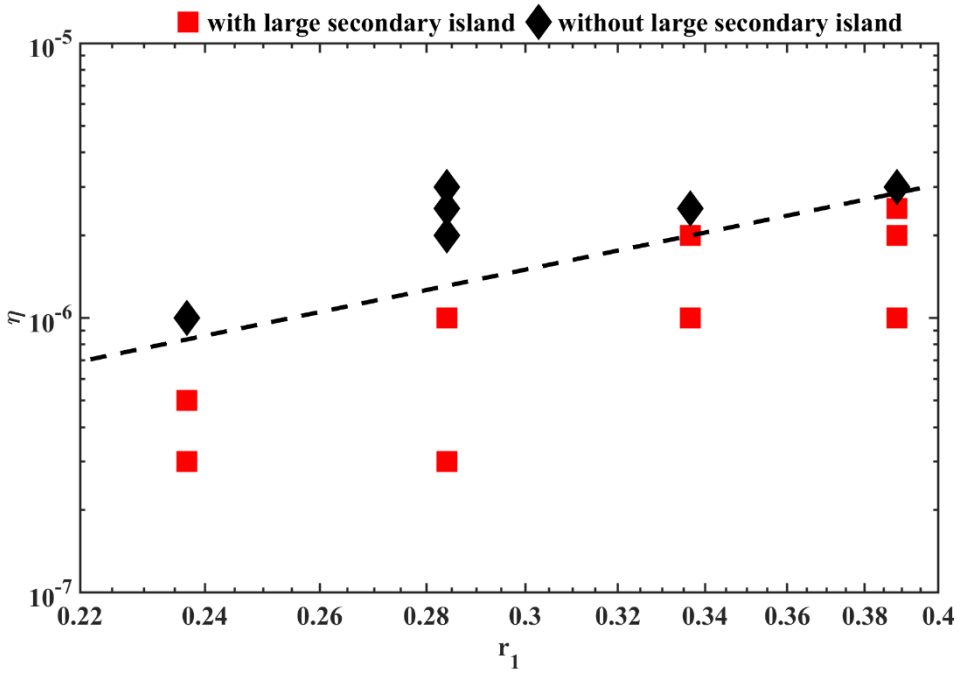

Figure 15 The influence of the location of the q=1 resonant surface and the resistivity on plasmoid formation. The red square/the black diamond represents with/without large secondary island formation in this simulation.

IV. Discussions and conclusions

Through the 3D toroidal nonlinear full-MHD simulations, we find that, with a relatively low resistivity, the secondary tearing instability can occur inside the thin current sheet and finally leads to the formation of a large secondary island. If the secondary island is sufficiently large, it can prevent the further development of the resistive kink mode and causes that the kink-driven reconnection ceases before the whole flux inside the mix region has been reconnected, i.e., the so-called incomplete reconnection occurs. If the secondary island is small, the main m/n=1/1 magnetic island can still grow up to occupy the whole core region and leads to complete reconnection. The maximum width of the secondary island increases with decreasing plasma resistivity.

Although these results are qualitatively the same as those in Ref. [31], the critical resistivity for plasmoid formation is largely different. We find that this is mainly due to the large aspect ratio assumptions adopted in the periodic cylindrical geometry. With large aspect ratios, our results can convergence to Yu's results. However, with the aspect ratio of real Tokamaks, the critical resistivity can be one magnitude larger than that with large aspect ratio assumptions. By using the Fourier transform method, we find that the high n modes are harder to develop in Tokamaks with large aspect ratios. This is why the critical resistivity for large secondary island formation decreases with increasing aspect ratios.

We have also found that the plasma viscosity, the radial location, and the local magnetic shear of the q=1 resonant surface can significantly influence the critical resistivity η_{crit} for plasmoid formation. The critical resistivity can change more than one magnitude in the scanning range of these parameters. For example, the critical resistivity is $\eta_{crit} = 3\times10^{-6}$ for the case with ν=1.0×10^{-7} while $\eta_{crit} = 5\times10^{-7}$ with ν=3.0×10^{-6}. The critical resistivity decreases with increasing plasma viscosity, and the magnetic shear on the q=1 resonant surface, or with decreasing radial locations of the q=1 resonant surface.

Acknowledgment

This work is supported by the National MCF Energy R&D Program No. 2019YFE03090500, the National Natural Science Foundation of China under Grant No. 12005185, 11775188, and 11835010, Fundamental Research Fund for Chinese Central Universities No. 2021FZZX003-03-02.

Reference:

[1] R.S. Steinolfson, G.V. Hoven, Nonlinear evolution of the resistive tearing mode, 27 (1984) 1207-1214.

[2] A. Bhattacharjee, Y.-M. Huang, H. Yang, B. Rogers, Fast reconnection in high-Lundquist-number plasmas due to the plasmoid Instability, Physics of Plasmas, 16 (2009) 112102.

[3] N.F. Loureiro, A.A. Schekochihin, S.C. Cowley, Instability of current sheets and formation of plasmoid chains, 14 (2007) 100703.

[4] R. Samtaney, N.F. Loureiro, D.A. Uzdensky, A.A. Schekochihin, S.C. Cowley, Formation of Plasmoid Chains in Magnetic Reconnection, Physical Review Letters, 103 (2009) 105004.

[5] N.F. Loureiro, D.A. Uzdensky, Magnetic reconnection: from the Sweet–Parker model to stochastic plasmoid chains, Plasma Physics and Controlled Fusion, 58 (2015) 014021.

[6] L. Comisso, D. Grasso, Visco-resistive plasmoid instability, 23 (2016) 032111.

[7] L. Comisso, M. Lingam, Y.-M. Huang, A. Bhattacharjee, General theory of the plasmoid instability, 23 (2016) 100702.

[8] E. Papini, S. Landi, L.D. Zanna, Fast Magnetic Reconnection: Secondary Tearing Instability and Role of the Hall Term, The Astrophysical Journal, 885 (2019) 56.

[9] Y.-M. Huang, A. Bhattacharjee, B.P. Sullivan, Onset of fast reconnection in Hall magnetohydrodynamics mediated by the plasmoid instability, 18 (2011) 072109.

[10] W. Daughton, V. Roytershteyn, B.J. Albright, H. Karimabadi, L. Yin, K.J. Bowers, Transition from collisional to kinetic regimes in large-scale reconnection layers, Physical Review Letters, 103 (2009)

065004.
[11] Y.-M. Huang, A. Bhattacharjee, TURBULENT MAGNETOHYDRODYNAMIC RECONNECTION MEDIATED BY THE PLASMOID INSTABILITY, The Astrophysical Journal, 818 (2016) 20.
[12] M.J. Nemati, Z.-X. Wang, L. Wei, Dynamics of the Plasmoid-unstable Regime in Different Multiple-current Plasmas, The Astrophysical Journal, 835 (2017) 191.
[13] Z.W. Ma, A. Bhattacharjee, Sudden disruption of a thin current sheet in collisionless Hall magnetohydrodynamics due to secondary tearing and coalescence instabilities, 26 (1999) 3337-3340.
[14] D.A. Uzdensky, N.F. Loureiro, A.A. Schekochihin, Fast Magnetic Reconnection in the Plasmoid-Dominated Regime, Physical Review Letters, 105 (2010) 235002.
[15] S. Zenitani, T. Miyoshi, Plasmoid-dominated Turbulent Reconnection in a Low-β Plasma, The Astrophysical Journal, 894 (2020) L7.
[16] P. Kumar, J.T. Karpen, S.K. Antiochos, P.F. Wyper, C.R. DeVore, First Detection of Plasmoids from Breakout Reconnection on the Sun, The Astrophysical Journal, 885 (2019) L15.
[17] S. Majeski, H. Ji, J. Jara-Almonte, J. Yoo, Guide field effects on the distribution of plasmoids in multiple scale reconnection, 28 (2021) 092106.
[18] Z.W. Ma, L.C. Wang, L.J. Li, Reconnection dynamics with secondary tearing instability in compressible Hall plasmas, 22 (2015) 062104.
[19] S. Günter, Q. Yu, K. Lackner, A. Bhattacharjee, Y.M. Huang, Fast sawtooth reconnection at realistic Lundquist numbers, Plasma Physics and Controlled Fusion, 57 (2015) 014017.
[20] W. Guo, J. Ma, Q. Yu, Numerical study on nonlinear growth of m/n = 3/1 double tearing mode in high Lundquist number regime, Plasma Physics and Controlled Fusion, 61 (2019) 075011.
[21] W. Guo, J. Ma, Z. Yu, Multiple secondary islands formation in nonlinear evolution of double tearing mode simulations, Physics of Plasmas, 24 (2017) 032115.
[22] J. Ma, W. Guo, Z. Yu, Q. Yu, Effect of plasmoids on nonlinear evolution of double tearing modes, Nuclear Fusion, 57 (2017) 126004.
[23] D.D. Sarto, M. Ottaviani, Secondary fast reconnecting instability in the sawtooth crash, 24 (2017) 012102.
[24] T. Akramov, H. Baty, Non-linear growth of double tearing mode: Explosive reconnection, plasmoid formation, and particle acceleration, Physics of Plasmas, 24 (2017) 082116.
[25] F. Ebrahimi, R. Raman, Plasmoids Formation During Simulations of Coaxial Helicity Injection in the National Spherical Torus Experiment, Physical Review Letters, 114 (2015) 205003.
[26] F. Ebrahimi, Dynamo-driven plasmoid formation from a current-sheet instability, 23 (2016) 120705.
[27] A. Mao, Z. Wang, X. He, X. Wang, Nonlinear evolution and secondary island formation of the double tearing mode in a hybrid simulation, Plasma Science and Technology, 23 (2021) 035103.
[28] Z.W. Ma, A. Otto, L.C. Lee, Core magnetic field enhancement in single X line, multiple X line and patchy reconnection, 99 (1994) 6125-6136.

[29] B. Coppi, R. Galvao, R. Pellat, M. Rosenbluth, P. Rutherford, Resistive internal kink modes, Fizika Plazmy, 2 (1976) 961-966.
[30] G. Ara, B. Basu, B. Coppi, G. Laval, M. Rosenbluth, B. Waddell, Magnetic reconnection and m= 1 oscillations in current carrying plasmas, Annals of Physics, 112 (1978) 443-476.
[31] Q. Yu, S. Günter, K. Lackner, Formation of plasmoids during sawtooth crashes, Nuclear Fusion, 54 (2014) 072005.
[32] B. Kadomtsev, Disruptive instability in Tokamaks(helical plasma motions), Soviet Journal of Plasma Physics, 1 (1975) 389-391.
[33] K. McGuire, V. Arunasalam, C.W. Barnes, M.G. Bell, M. Bitter, R. Boivin, N.L. Bretz, R. Budny, C.E. Bush, A. Cavallo, T.K. Chu, S.A. Cohen, P. Colestock, S.L. Davis, D.L. Dimock, H.F. Dylla, P.C. Efthimion, A.B. Ehrhrardt, R.J. Fonck, E. Fredrickson, H.P. Furth, G. Gammel, R.J. Goldston, G. Greene, B. Grek, L.R. Grisham, G. Hammett, R.J. Hawryluk, H.W. Hendel, K.W. Hill, E. Hinnov, D.J. Hoffman, J. Hosea, R.B. Howell, H. Hsuan, R.A. Hulse, A.C. Janos, D. Jassby, F. Jobes, D.W. Johnson, L.C. Johnson, R. Kaita, C. Kieras-Phillips, S.J. Kilpatrick, P.H. LaMarche, B. LeBlanc, D.M. Manos, D.K. Mansfield, E. Mazzucato, M.P. McCarthy, M.C. McCune, D.H. McNeill, D.M. Meade, S.S. Medley, D.R. Mikkelsen, D. Monticello, R. Motley, D. Mueller, J.A. Murphy, Y. Nagayama, D.R. Nazakian, E.B. Neischmidt, D.K. Owens, H. Park, W. Park, S. Pitcher, A.T. Ramsey, M.H. Redi, A.L. Roquemore, P.H. Rutherford, G. Schilling, J. Schivell, G.L. Schmidt, S.D. Scott, J.C. Sinnis, J. Stevens, B.C. Stratton, W. Stodiek, E.J. Synakowski, W.M. Tang, G. Taylor, J.R. Timberlake, H.H. Towner, M. Ulrickson, S.v. Goeler, R. Wieland, M. Williams, J.R. Wilson, K.L. Wong, M. Yamada, S. Yoshikawa, K.M. Young, M.C. Zarnstorff, S.J. Zweben, High-beta operation and magnetohydrodynamic activity on the TFTR tokamak, Physics of Fluids B: Plasma Physics, 2 (1990) 1287-1290.
[34] A. Letsch, H. Zohm, F. Ryter, W. Suttrop, A. Gude, F. Porcelli, C. Angioni, I. Furno, Incomplete reconnection in sawtooth crashes in ASDEX Upgrade, Nuclear Fusion, 42 (2002) 1055.
[35] V. Igochine, J. Boom, I. Classen, O. Dumbrajs, S. Günter, K. Lackner, G. Pereverzev, H. Zohm, A.U. Team, Structure and dynamics of sawteeth crashes in ASDEX Upgrade, Physics of Plasmas, 17 (2010) 122506.
[36] I. Furno, C. Angioni, F. Porcelli, H. Weisen, R. Behn, T.P. Goodman, M.A. Henderson, Z.A. Pietrzyk, A. Pochelon, H. Reimerdes, E. Rossi, Understanding sawtooth activity during intense electron cyclotron heating experiments on TCV, Nuclear Fusion, 41 (2001) 403.
[37] V. Igochine, O. Dumbrajs, H. Zohm, A. Flaws, t.A.U. Team, Stochastic sawtooth reconnection in ASDEX Upgrade, Nuclear Fusion, 47 (2006) 23-32.
[38] H. Soltwisch, Measurement of current-density changes during sawtooth activity in a tokamak by far-infrared polarimetry (invited), 59 (1988) 1599-1604.
[39] W. Zhang, S.C. Jardin, Z.W. Ma, A. Kleiner, H.W. Zhang, Linear and nonlinear benchmarks between the CLT code and the M3D-C1 code for the 2/1 resistive tearing mode and the 1/1 resistive kink mode, Computer Physics Communications, DOI https://doi.org/10.1016/j.cpc.2021.108134(2021) 108134.

[40] H.W. Zhang, J. Zhu, Z.W. Ma, G.Y. Kan, X. Wang, W. Zhang, Acceleration of three-dimensional Tokamak magnetohydrodynamical code with graphics processing unit and OpenACC heterogeneous parallel programming, International Journal of Computational Fluid Dynamics, 33 (2019) 393-406.
[41] L. Duan, X. Wang, X. Zhong, A high-order cut-cell method for numerical simulation of hypersonic boundary-layer instability with surface roughness, Journal of Computational Physics, 229 (2010) 7207-7237.
[42] C. Cheng, M. Chance, NOVA: A nonvariational code for solving the MHD stability of axisymmetric toroidal plasmas, Journal of Computational Physics, 71 (1987) 124-146.
[43] W. Suttrop, T. Eich, J.C. Fuchs, S. Günter, A. Janzer, A. Herrmann, A. Kallenbach, P.T. Lang, T. Lunt, M. Maraschek, R.M. McDermott, A. Mlynek, T. Pütterich, M. Rott, T. Vierle, E. Wolfrum, Q. Yu, I. Zammuto, H. Zohm, First Observation of Edge Localized Modes Mitigation with Resonant and Nonresonant Magnetic Perturbations in ASDEX Upgrade, Physical Review Letters, 106 (2011) 225004.
[44] Q. Yu, S. Günter, K. Lackner, E. Strumberger, V. Igochine, Numerical study on toroidal mode coupling and triggering of neoclassical tearing modes by sawteeth, Nuclear Fusion, 59 (2019) 106053.